Supplement of Atmos. Meas. Tech. Discuss., 8, 3803–3850, 2015
http://www.atmos-meas-tech-discuss.net/8/3803/2015/
doi:10.5194/amtd-8-3803-2015-supplement
© Author(s) 2015. CC Attribution 3.0 License.

Atmospheric Measurement Techniques Discussions

Supplement of

Detailed characterizations of a Comparative Reactivity Method (CRM) instrument: experiments vs. modelling

V. Michoud et al.

Correspondence to:

Supplementary material 1: Comparison between measured and calculated total OH reactivity values for two different gas mixtures: Non-Methane Hydrocarbons (NMHCs) and Oxygenated VOCs (OVOCs)

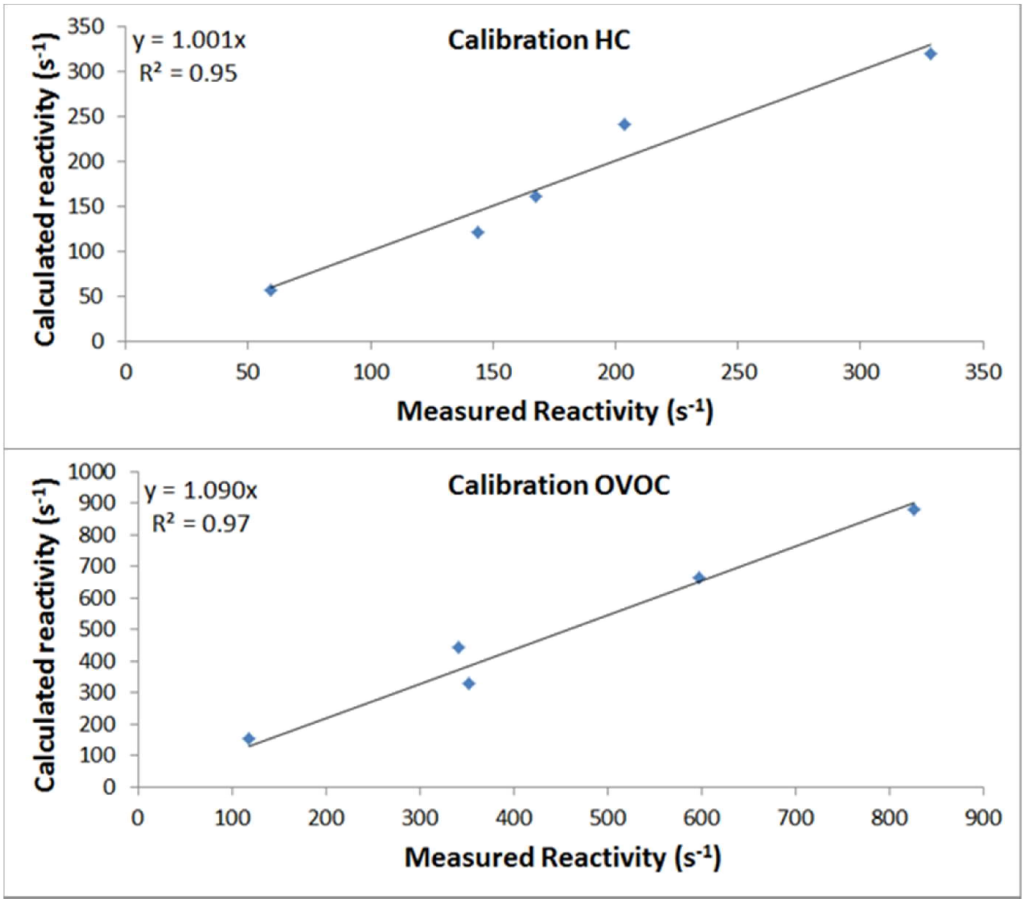

Figure S1: Scatter plot of calculated-to-measured OH reactivity for two different gas mixtures: NMHCs (top panel) and OVOCs (bottom panel). Chemical compositions of these mixtures are given in table S1. The measured OH reactivity corresponds to the total OH reactivity measured by MD-CRM and corrected for the changes in humidity between C2 and C3 and for the deviation from pseudo first order kinetics. Correction for dilution is not performed since it is taken into account in the calculated OH reactivity.

Table S1: Chemical composition of the OVOC and NMHC cylinders used for the tests presented above.

Species OVOC cylinder	Mixing ratios (ppm)	Species HC cylinder	Mixing ratios (ppm)
Methanol	2.15	Acetonitrile	0.63
Acetaldehyde	1.43	Acrylonitrile	0.51
Acetone	4.50	Benzene	0.96
Methyl Ethyl Ketone	1.40	Toluene	0.91
2-Methylfuran	1.51	EthylBenzene	0.80
Acrolein	1.48	1,2,4-TrimethylBenzene	0.52
Methacrolein	1.65	Styrene	0.71
Methyl Vinyl Ketone	1.54	Alpha-Pinene	1.07
3-Methyl-2-buten-1-ol	0.60	Methyl Sulfur	1.14

Table S2: Reactions included in the simple mechanism (see section 3.1 of the main manuscript).

Reactions	Bimolecular rate constants (cm^3 $molecules^{-1}$ s^{-1})
$H + O_2 = HO_2$	$7.5\ 10^{-11}$
$OH + VOC = RO_2$	$5.0\ 10^{-12}$
$OH + Pyrrole = RO_2$	$1.2\ 10^{-10}$
$RO_2 + RO_2 =$	$3.4\ 10^{-13}$
$RO_2 + HO_2 =$	$5.2\ 10^{-12}$
$RO_2 + NO = RO+NO_2$	$7.7\ 10^{-12}$
$RO + O_2 = HO_2$	$1.9\ 10^{-15}$

In addition of these organic reactions, inorganic reactions from IUPAC 2001 mechanism have been added, leading to a chemical mechanism of 42 reactions in total.

Supplementary material 2: Experiments performed to investigate NO interferences in the presence of VOC reactivity – addition of ethane and isoprene

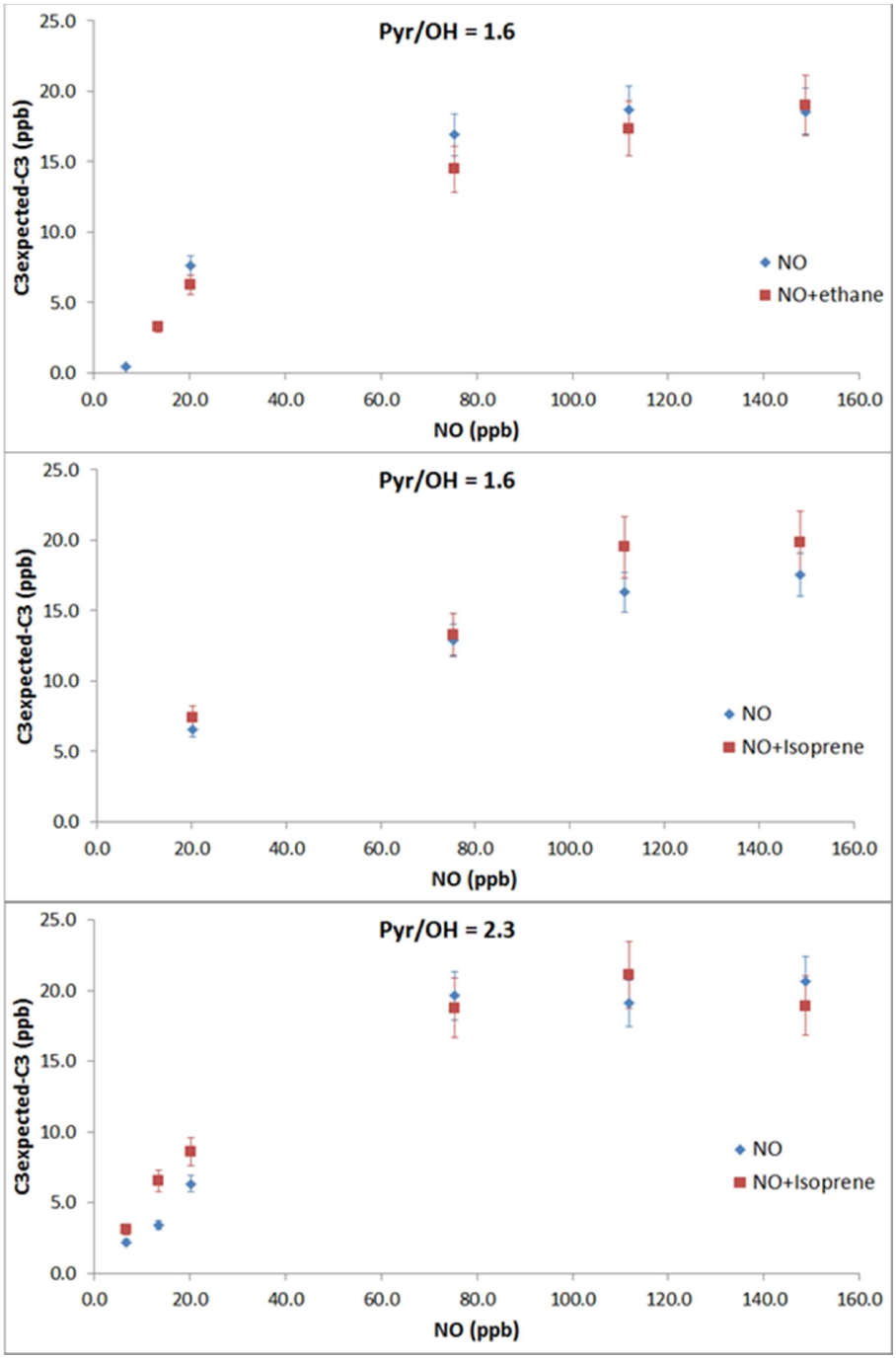

Figure S2: Experimental results of the changes in C3 (ΔC3 = C3 expected – C3 measured) as a function of NO mixing ratios in the reactor with and without addition of a VOC. These experiments have been conducted with two different standards (ethane and isoprene) selected for their different kinetic rate constants with OH (2.4 10^{-13} and 1.0 10^{-10} cm^3 $molecules^{-1}$ s^{-1}, respectively). The concentrations added were 3.7 ppm and 14.6 ppb for ethane and isoprene, respectively, leading to calculated OH reactivity values of 22.2 s^{-1} and 36.6 s^{-1}, respectively.

Experiments made using isoprene have been conducted at two different Pyrrole-to-OH ratios (1.6 and 2.3) to test the influence of this parameter on NO interferences in the presence of a standard.

The differences observed in NO interferences in the presence of a standard seem to be within experimental uncertainties (9-11%), except for low concentrations of NO for the experiment at a pyrrole-to-OH ratio of 2.3 for Isoprene. No clear influence of the Pyrrole-to-OH ratio or of the VOC reactivity has been found on the amplitude of the NO interference.

Supplementary material 3: Comparison between real and apparent Pyrrole-to-OH ratios

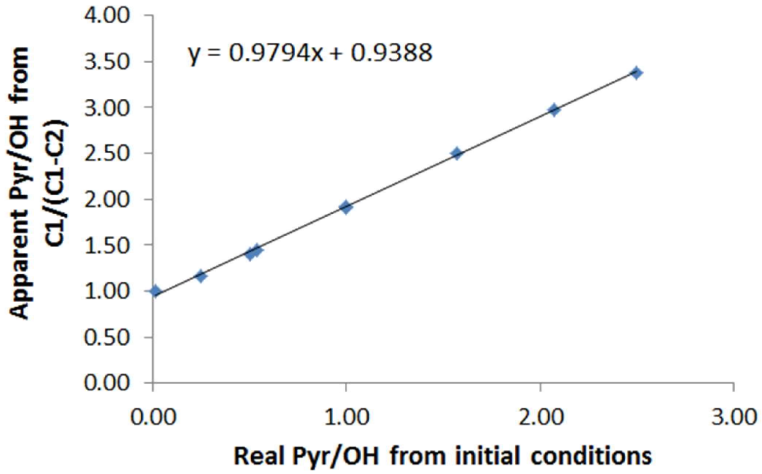

Figure S3: Comparison between real and apparent pyrrole-to-OH ratios for simulations conducted under dry conditions with the simple mechanism presented in section 3.1 of the main manuscript. Apparent pyrrole-to-OH ratios are calculated using Eq. (2), where C1 is the initial concentration of pyrrole and C2 the final concentration of pyrrole when all the OH has been reacted in the simulations. This apparent ratio provides the amount of OH that has reacted with pyrrole in the model.

This figure shows that running the CRM instrument at an apparent pyrrole-to-OH ratio of 1.5-2.5 leads to a real ratio of approximately 0.5-1.5. The main manuscript and this supplementary material always refer to the apparent pyrrole-to-OH ratio since it is the measurable quantity.

Supplementary material 4: Experimental measurements of the OH mixing ratio inside the CRM reactor

Experiments have been conducted to determine the OH mixing ratio inside the reactor. A large mixing ratio of isoprene (3 ppm) was injected inside the reactor with (mercury lamp ON) or without (mercury lamp OFF) OH production and was monitored by the PTR-ToFMS instrument at m/z 69. Simulations have been conducted using MCM to ensure that this level of isoprene allows scavenging more than 97% of OH in the reactor. The OH mixing ratio

present within the reactor can be derived from the decrease of isoprene when the OH production is turned ON. This OH mixing ratio, referred as "OH experiment", was determined at two different pyrrole-to-OH ratios of 1.6 and 3.8. The level of OH quantified experimentally from (C1-C2), i.e. the amount of OH reacting with pyrrole, is referred as "OH estimated CRM" and is compared to the total mixing ratio of OH determined experimentally. In addition, the OH mixing ratio necessary to reproduce the experimental C1-C2 modulation with the model is referred as "OH model". The three OH mixing ratios are shown in Fig. S4.

As seen with the model (see supplementary S3), the OH mixing ratio in the reactor is higher than the level determined from the C1-C2 modulation but only slightly lower (~10-20%) than the OH level set in the model (within experimental uncertainties). However, the fact that the isoprene injected inside the reactor is not high enough to scavenge all the OH cannot be excluded, and some OH might react with the HO_2 present in the reactor leading to a slight underestimation of OH levels determined experimentally. From these results, we consider that the OH mixing ratio set in the model to reproduce the experimental C1-C2 modulation is representative of the real mixing ratio in the reactor.

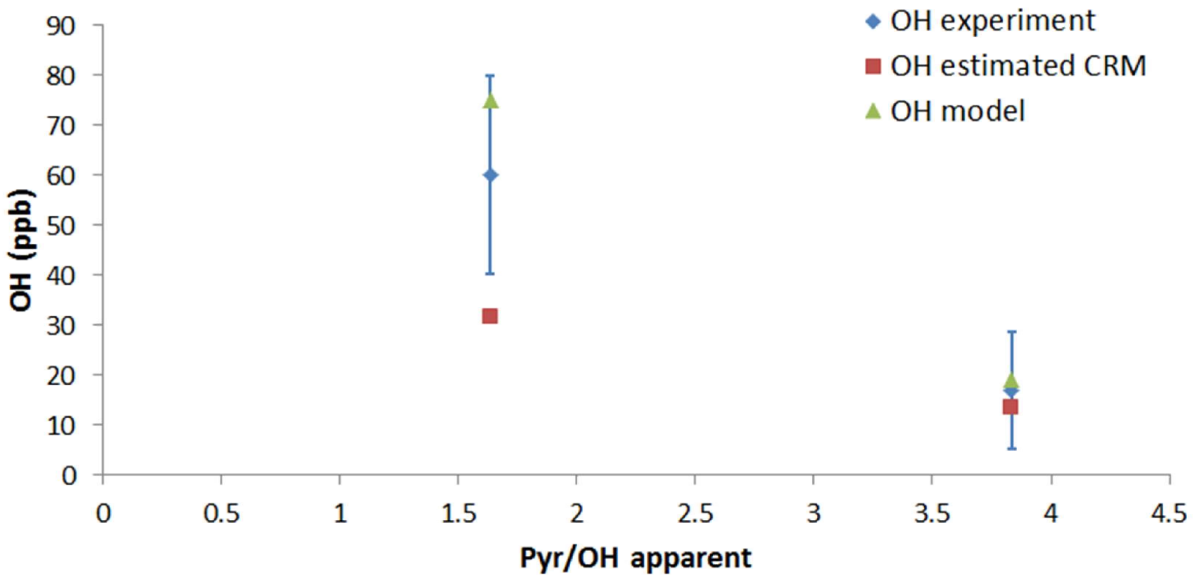

Figure S4: Comparison between OH mixing ratios determined experimentally ("OH experiment", blue diamonds), calculated from the C1-C2 modulation ("OH estimated CRM", red squares), and estimated from the model ("OH model", green triangles) at two different apparent pyrrole-to-OH ratios (1.6 and 3.8). Error bars are the precision of the experimental determination. Large error bars (33-68%) are found since OH determinations correspond to differences of tens of ppb for initial mixing ratios of isoprene of approximately 3 ppm.

Supplementary material 5: Influence of humidity on the NO interference derived from the simulations

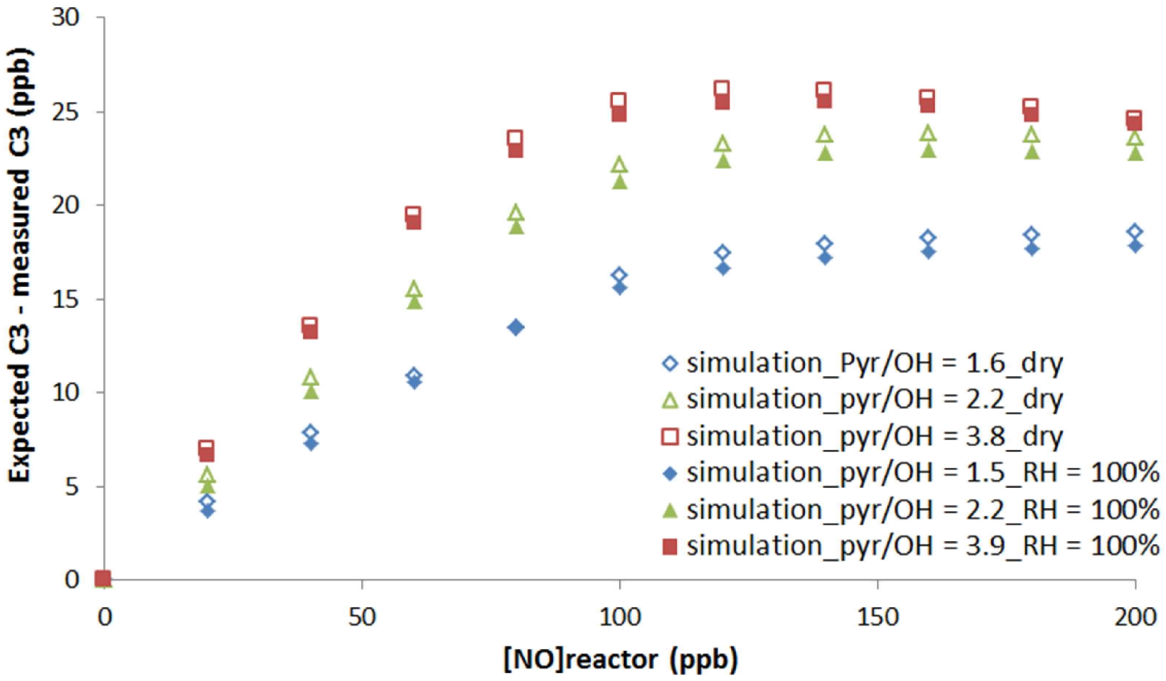

Figure S5: Comparison between simulations of NO interferences under dry (open symbols) and wet (filled symbols) conditions at three different pyrrole-to-OH ratios of 1.5-1.6 (blue diamonds), 2.2 (green triangles), and 3.8-3.9 (red squares). Simulations have been performed using the simple mechanism and wet conditions correspond to a relative humidity of 100%.

A slight decrease of ΔC3 is observed at all pyrrole-to-OH ratios. This can be explained by an enhancement of the rate of the HO_2 + HO_2 reaction in the presence of water, reducing the secondary formation of OH, hence the NO interference.

Supplementary material 6: Influence of standard addition on the NO interference derived from the simulations

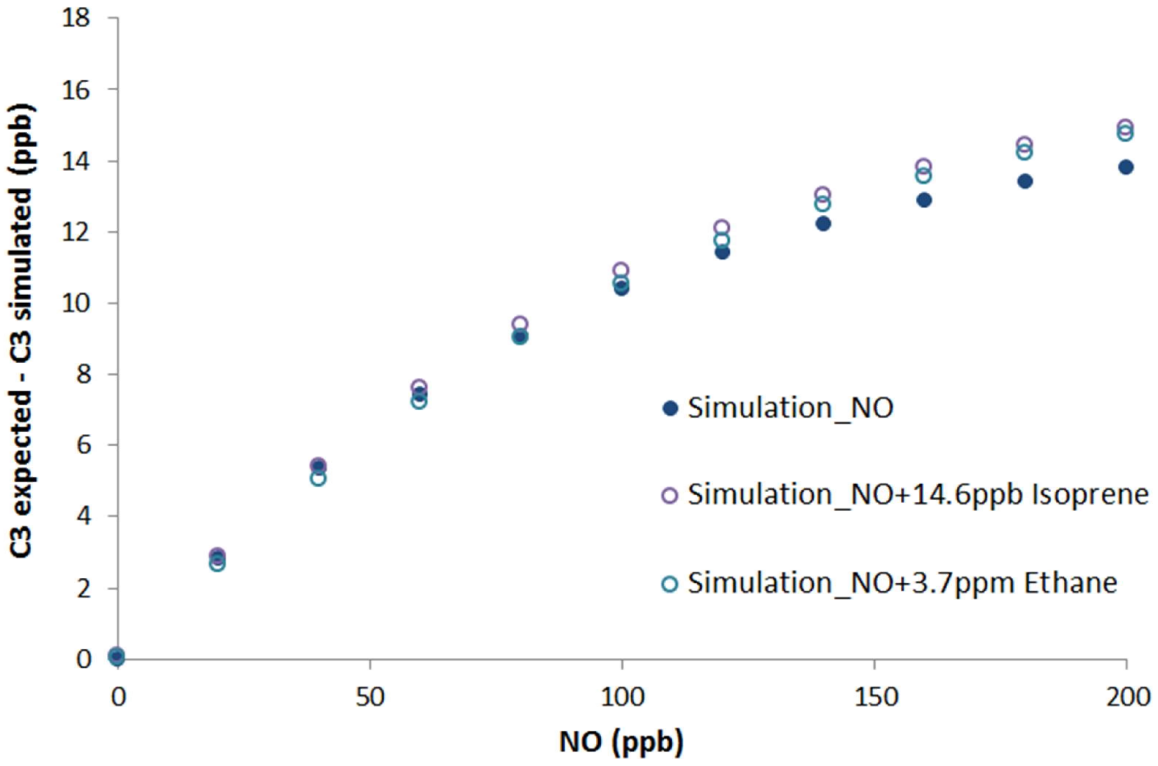

Figure S6: Simulated changes in C3 mixing ratios (ΔC3 = C3 expected – C3 simulated) as a function of NO mixing ratios. This figure shows simulations made with (open circles) and without (filled circles) a standard addition. These simulations have been conducted with the MCM mechanism at an apparent pyrrole-to-OH ratio of 1.4. The standards are isoprene (14.6 ppb) and ethane (3.7 ppm), leading to additional OH reactivities of 36.6 s^{-1} and 22.2 s^{-1}, respectively.

Supplementary material 7: Influence of the bimolecular rate constant on the correction factor

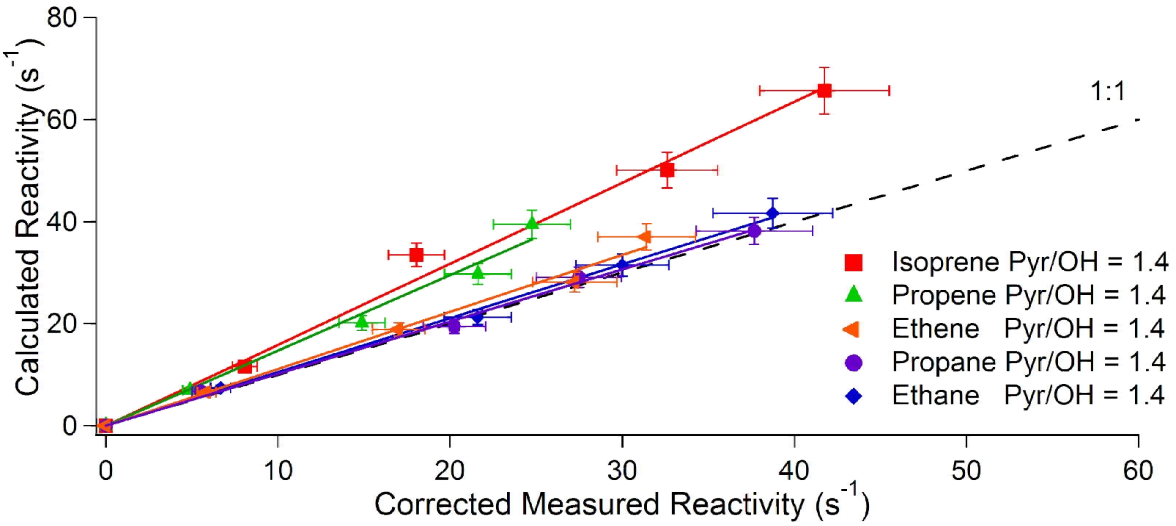

Figure S7: Experimental investigations of the bias caused by a deviation from pseudo first-order kinetics. Comparison of calculated (true) reactivity to measured reactivity during standard additions into the reactor. Results from the addition of five different standards (Isoprene: red squares, Propene: green triangles, Ethene: orange triangles, Propane: purple circles, and Ethane: blue diamonds), characterized by different reaction rate constants with OH ($1.0\ 10^{-10}$, $2.9\ 10^{-11}$, $8{,}5\times10^{-12}$, 1.09×10^{-12}, and $2.4\ 10^{-13}$ cm^3 $molecules^{-1}$ s^{-1}, respectively), at a pyrrole-to-OH ratio of 1.4.

Supplementary material 8: Potential influence of reactant segregation on the simulations

One hypothesis to explain the differences observed between measurements and simulations for the correction associated to a deviation from pseudo first-order kinetics is that a segregation between the reactants coming from the two injectors (OH and HO_2 on one side and pyrrole + reactive trace gases on the other side) impacts the chemical reaction rates inside the reactor. To account for this segregation (i.e. inhomogeneity in the reactor), we doubled the reaction rate constants of cross- and self-reactions of radicals (i.e. HO_2+OH and HO_2+HO_2) assuming that these reactions are favored by the inhomogeneity inside the reactor, all the radicals being injected from the same injector. Figure S8 shows the comparison between base simulations and simulations conducted to evaluate the potential impact of reactant segregation as a function of the pyrrole-to-OH ratio. Laboratory derived correction factors are also shown. Simulations where segregation is added do not allow reconciling simulations and measurements since they even lead to a larger difference.

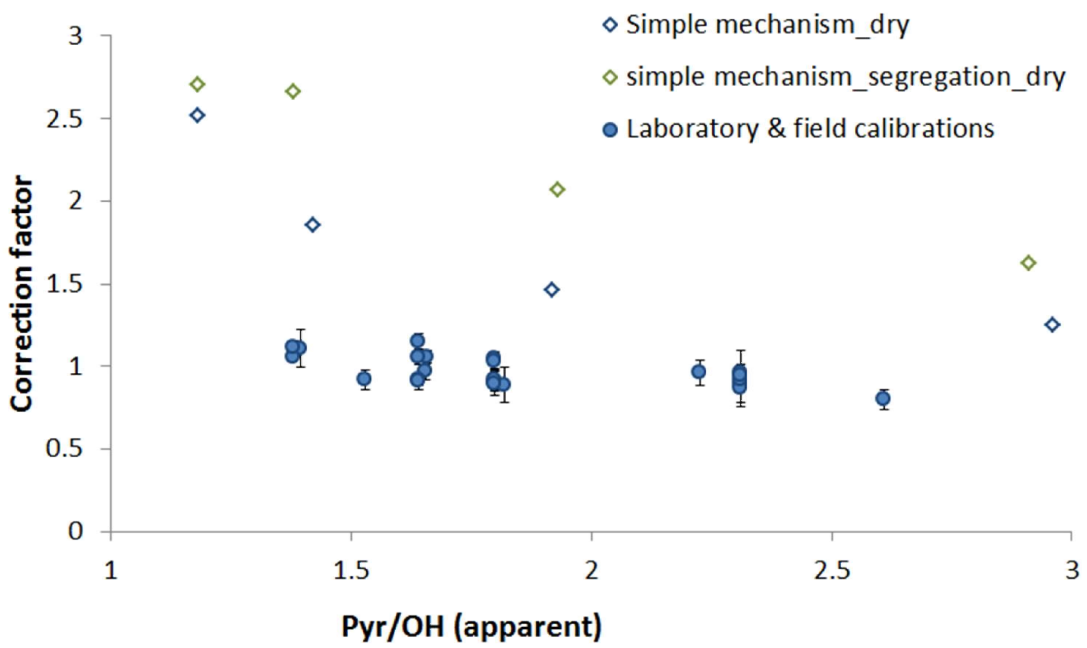

Figure S8: Comparison of the simulated and measured correction factors as a function of the Pyrrole-to-OH ratio. The measured correction factors (blues circles), as well as error bars, are the same than in Fig. 7. The simulated correction factors stem from the simulations conducted using the base simple mechanism (blue open diamonds) and the modified simple mechanism (green open diamonds).

Supplementary material 9: Potential influence of RO_2+OH reactions on the simulations

A recent study has proposed the reaction of CH_3O_2 with OH as a potential sink of CH_3O_2 in the remote atmosphere (Fittschen et al., 2014). Since radical concentrations in the CRM reactor are high, radical-radical reactions have an important impact on the CRM measurements. We have, therefore, tested the addition of the reaction between peroxy radicals and OH in the simple mechanism, assuming a reaction rate constant similar to the one of CH_3O_2 determined by Fittschen et al. (2014). Figure S9 shows the comparison between the correction factors derived from base simulations and simulations including the fast RO_2+OH reactions as a function of the pyrrole-to-OH ratio. The addition of this reaction in the chemical mechanism leads to an increase of the correction factor and does not allow reconciling simulations and measurements.

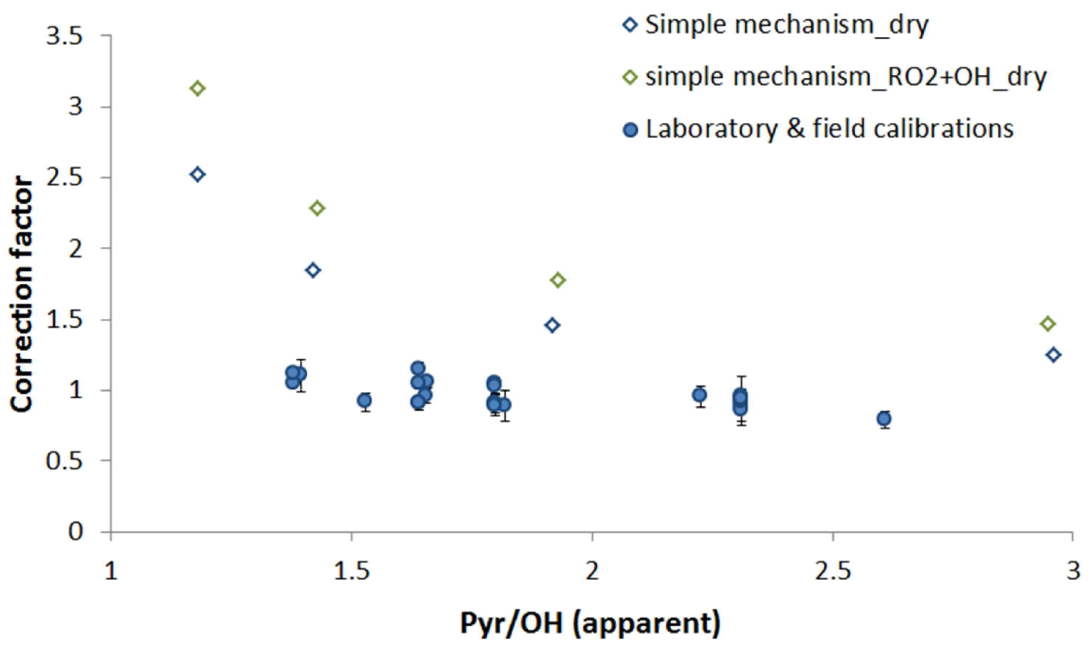

Figure S9: Comparison of the simulated and measured correction factors as a function of the Pyrrole-to-OH ratio. The measured correction factors (blues circles), as well as error bars, are the same than in Fig. 7. The simulated correction factors stem from the simulations conducted using the base simple mechanism (blue open diamonds) and the modified simple mechanism (green open diamonds). The reaction rate constant for RO_2+OH has been set to 2.0 10^{-10} cm^3 $molecules^{-1}$ s^{-1}, corresponding to the rate constant of the reaction of CH_3O_2 + OH (Fittschen et al., 2014).

Supplementary material 10: Potential influence of uncertainties on radical-radical reaction rate constants on the simulations

From the two previous tests (S8-S9), it appears that enhancing radical-radical reaction rates tends to increase the correction factors derived from the simulations. One can imagine that an overestimation of reaction rate constants of these reactions can contribute to the discrepancies between measurements and simulations. To test the influence of the uncertainties on these reaction rate constants, simulations have been performed with a reduction of 20% and 50% of the reaction rate constant of HO_2+OH. Figure S10 shows the comparison between measured correction factors, base simulations, and simulations where a reduction of the reaction rate constant has been made. The decrease of the HO_2+OH reaction rate constant allows to decrease the modeled correction factors and to get a better agreement with experimental observations. However, a reduction of the rate constant by 20% is not sufficient to reconcile measurements and simulations. Even with a reduction of 50%, simulated correction factors are still slightly higher than the measurements. Furthermore, a 50% uncertainty on this reaction rate constant is not likely. Therefore, the uncertainty of reaction rate constants of radical-radical reactions cannot totally explain the discrepancies between simulations and measurements.

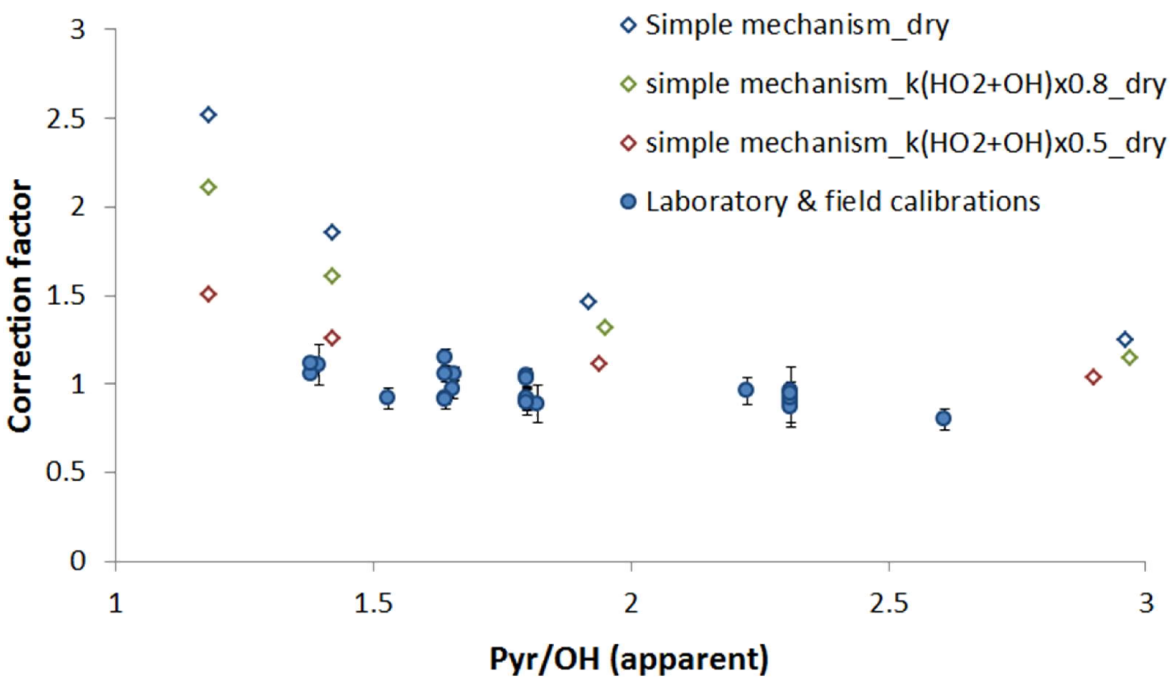

Figure S10: Comparison of the simulated and measured correction factors as a function of the Pyrrole-to-OH ratio. The measured correction factors (blues circles), as well as error bars, are the same than in Fig. 7. The simulated correction factors stem from the simulations conducted using the base simple mechanism (blue open diamonds) and the modified mechanism where the reaction rate constant of HO_2+OH has been reduced by 20% (green open diamonds) and 50% (red open diamonds).

Supplementary material 11: Potential influence of a higher proportion of HO_2 compared to OH on the simulations

In all the simulations presented in the main paper or above, we assumed a similar concentration of HO_2 compared to OH, since HO_2 is formed at a similar amount than OH by the photolysis of water. However, it is likely that a larger amount of OH radicals is lost on the walls of the injector compared to HO_2. Therefore, a HO_2–to-OH ratio higher than unity might be observed inside the reactor. The influence of a higher proportion of HO_2 compared to OH has been tested with the simple mechanism by setting initial HO_2 concentrations higher by 20% than OH concentrations.

Figure S11 shows the comparison between measured values, base simulations and simulations where constrained initial HO_2 concentrations are higher than OH concentrations by 20%. A higher proportion of HO_2 leads to higher simulated correction factors and does not allow reconciling the simulations with the measurements and even worsen the comparison.

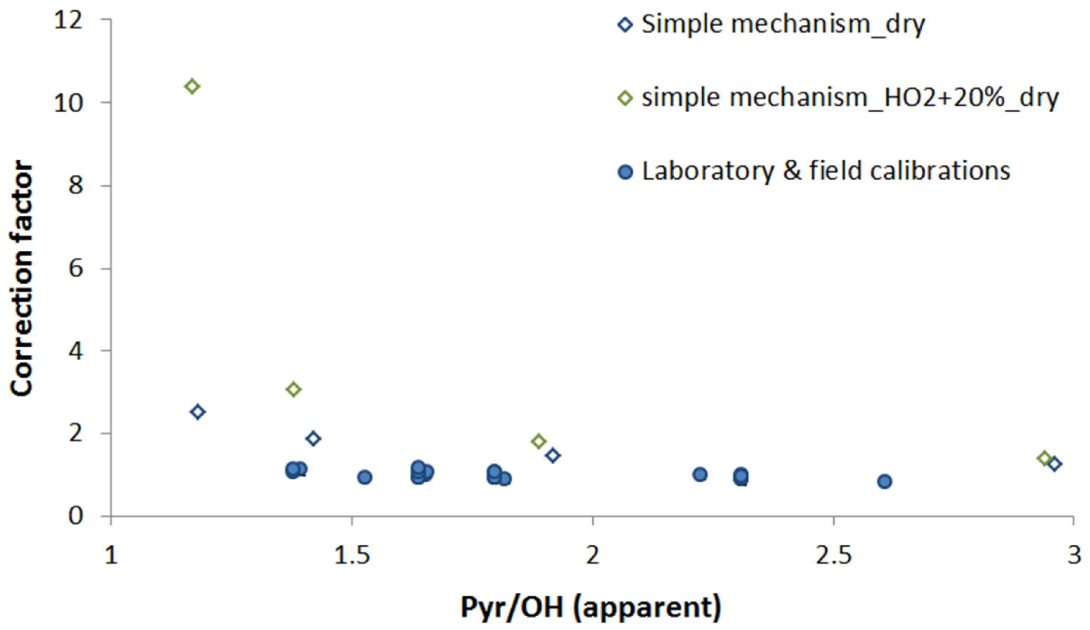

Figure S11: Comparison of simulated and measured correction factors as a function of the Pyrrole-to-OH ratio. The measured correction factors (blues circles), as well as error bars (hardly visible), are the same than in Fig. 7. The simulated correction factors stem from the simulations conducted using the base simple mechanism assuming the same concentration for OH and HO_2 (blue open diamonds) and runs where the proportion of HO_2 compared to OH has been raised by 20% (green open diamonds).

Supplementary material 12: Potential influence of the presence of O_3 inside the reactor on the simulations

All the simulations presented in this work have been performed without O_3. However, photolysis of O_2 from the mercury lamp emission may occur inside the reactor and may lead to the formation of a significant concentration of O_3. In this context, the influence of O_3 inside the reactor has been tested for both the pseudo first order correction and the NO artefact. The O_3 concentration has been constrained at 200 ppb in the simulations. The 200 ppb correspond to the mixing ratio measured using an ozone analyzer (Environnement-SA, model O3-42M) at the exhaust of the reactor under dry conditions and the lamp ON.

Figure S12.1 shows the comparison between measured pseudo first order correction factors, base simulations, and simulations where initial O_3 concentrations have been set to 200 ppb. The presence of O_3 in the simulations has almost no impact on simulated correction factors. This can be explained by the fact that the kinetic rate constant for the reaction between Pyrrole and O_3 is seven orders of magnitude lower than the rate constant for the reaction between Pyrrole and OH and that initial mixing ratios of O_3 are only a factor 2.3 to 19 higher than initial OH mixing ratios. Furthermore, these simulations indicate that the impact of the $O_3 + HO_2 \rightarrow$ OH reaction has only a small impact on CRM simulations, probably due to a slow reaction rate, even with high concentrations of HO_2 (27-220 ppb) and O_3 (200 ppb) inside the reactor.

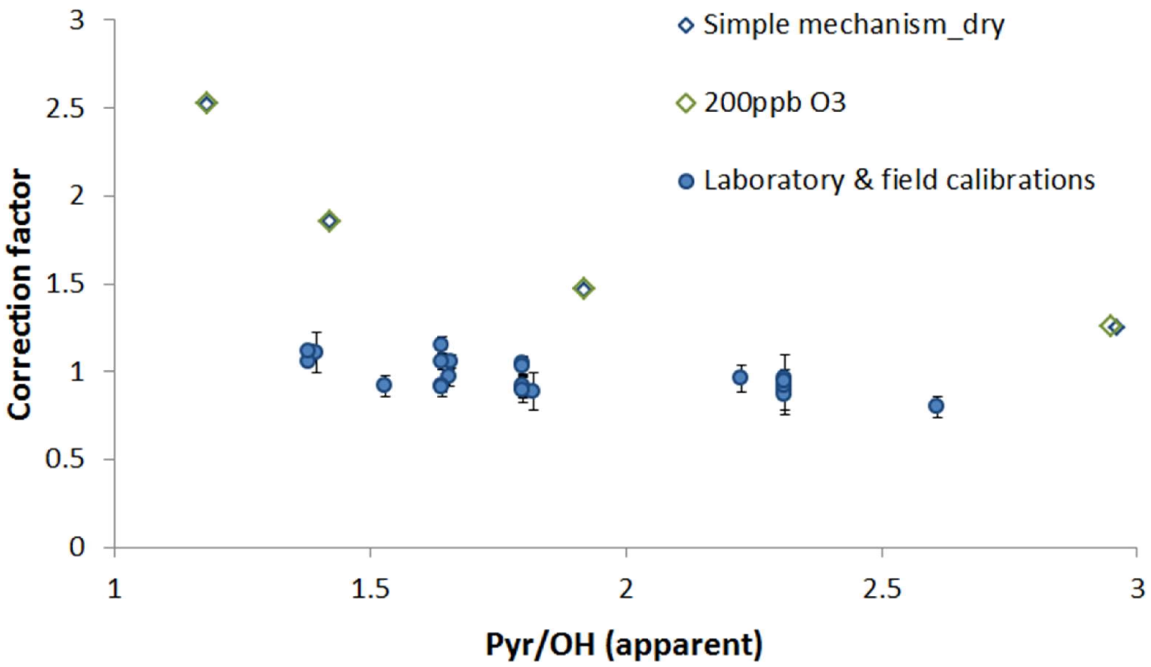

Figure S12.1: Comparison of simulated and measured correction factors as a function of the Pyrrole-to-OH ratio. The measured correction factors (blues circles), as well as error bars, are the same than in Fig. 7. The simulated correction factors stem from the simulations conducted using the base simple mechanism (blue open diamonds) and the modified mechanism where initial concentrations of O_3 have been set to 200 ppb (green open diamonds).

Figure S12.2 presents the comparison between experimental and simulated results of the NO artefact. Simulations have been performed using the base MCM mechanism and runs initialized with an O_3 mixing ratios of 200 ppb. The presence of 200 ppb of ozone in the simulations leads to a decrease of the NO artefact by approximately 2.5%, independently of the pyrrole-to-OH ratio.

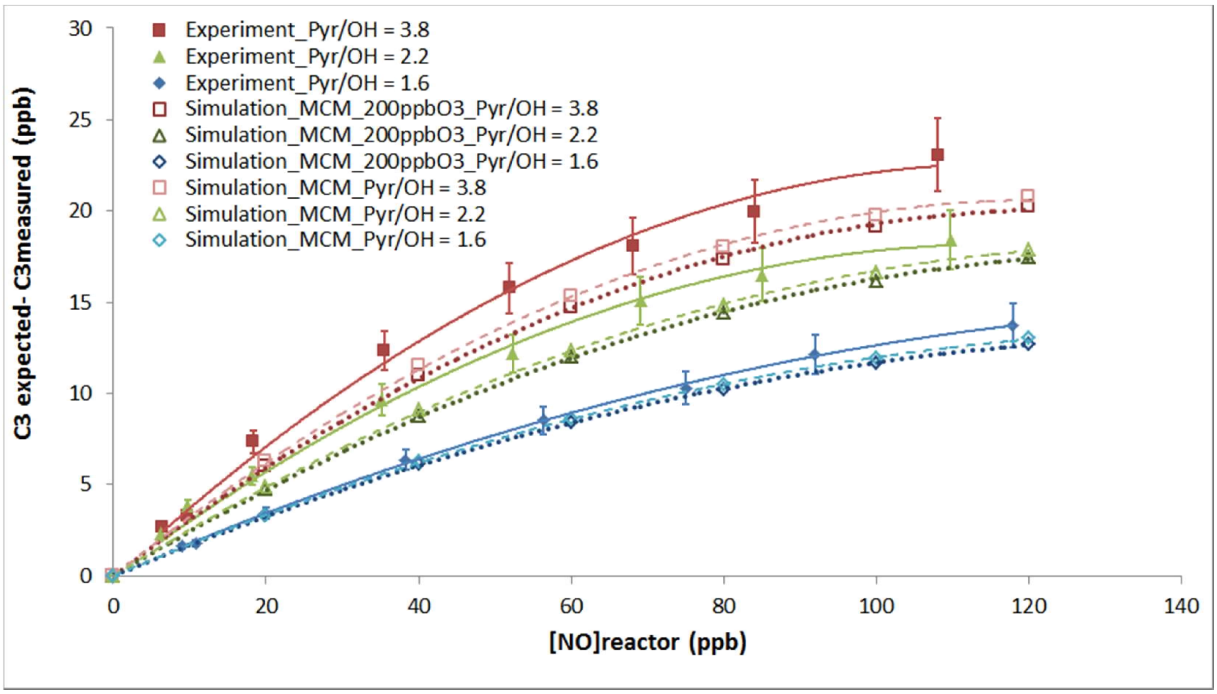

Figure S12.1: Comparison of laboratory observations to model simulations for the NO interference. Experimental (filled symbols and solid lines) and simulated (open symbols and dashed or dotted lines) results are shown for the changes in C3 (ΔC3 = C3 expected – C3 measured) as a function of NO mixing ratios in the reactor. The experimental values are the same than in Fig. 5. Model values are from simulations made using the base MCM mechanism (open lighter symbols and dashed lines) and the modified MCM mechanism where initial O_3 concentrations have been set to 200 ppb (open darker symbols and dotted lines).

Supplementary material 13: Potential influence of a lower proportion of HO_2 compared to OH on the simulations

As described in the supplement S12, high level of O_3 (~200 ppb) is produced inside the reactor from the photolysis of O_2. Therefore, the ozone produced can lead to a production of OH inside the reactor from its photolysis ($O_3 + h\nu \rightarrow O^1D + O_2$ followed by $O^1D + H_2O \rightarrow 2OH$). This OH source is free of HO_2 production. If a non-negligible fraction of OH present in the reactor comes from this OH source, then OH might be present in the reactor at a higher proportion than HO_2. Therefore, the influence of a lower proportion of HO_2 compared to OH has also been tested with the simple mechanism by setting initial HO_2 concentrations lower by 25% than OH concentrations.

Figure S13 shows the comparison between measured values, base simulations and simulations where constrained initial HO_2 concentrations are lower than OH concentrations by 25%. A lower proportion of HO_2 leads to lower simulated correction factors. However, it cannot totally explain the discrepancies. Furthermore, a lower proportion of HO_2 compared to OH is not likely since the photolysis of H_2O inside the injector will bring a larger amount of HO_2 compared to OH inside the reactor, which would partly compensate the absence of HO_2 production from O_3 photolysis. It is worth noting that a reduction of the proportion of HO_2

compared to OH by 25% would also result in a reduction of the NO artefact by approximately 6% using the MCM mechanism (not shown).

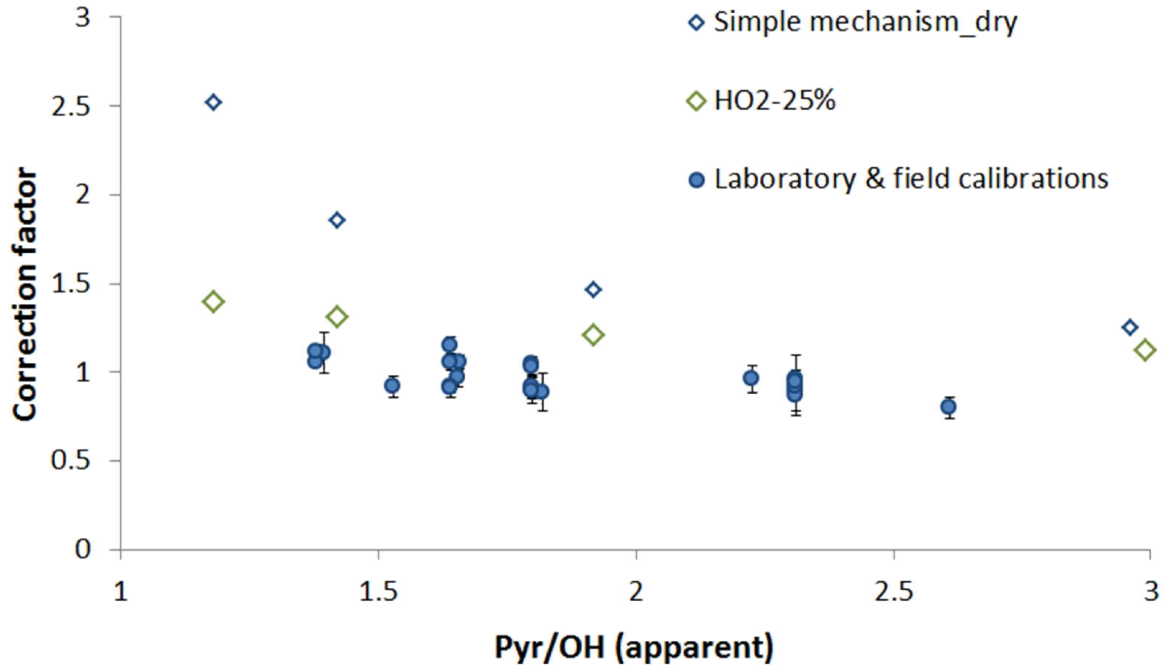

Figure S13: Comparison of simulated and measured correction factors as a function of the Pyrrole-to-OH ratio. The measured correction factors (blues circles) as well as error bars are the same than in Fig. 7. The simulated correction factors stem from the simulations conducted using the base simple mechanism assuming the same concentration for OH and HO_2 (blue open diamonds) and runs where the proportion of HO_2 was reduced by 25% compared to OH (green open diamonds).

Supplementary material 14: Assessment of the OH reactivity uncertainties

To assess the uncertainties of ambient OH reactivity measurements it is necessary to take into account errors associated to all the quantities involved in the OH reactivity calculations (Eq. 1), including the different corrections. When we include corrections, the final OH reactivity is calculated by the following equation:

$$k_{OH} = \frac{((C3 + \Delta C3) - (C2 + \Delta C2)}{(C1 - (C3 + \Delta C3))} \cdot k_p.C1.F.D$$

Where k_{OH} is the final total OH reactivity, C3, C2 and C1 the concentrations of pyrrole at different measurement steps (see the main manuscript), ΔC3 the change in C3 due to the NO interference, ΔC2 the change in C2 due to difference in RH between C2 and C3, k_p the reaction rate constant of pyrrole with OH, F the correction factor to apply for a deviation from pseudo first-order kinetics, and D the correction factor for dilution of ambient air inside the reactor.

Considering that only PTR-MS signals produce uncertainties in the determination of pyrrole concentrations, we can express the equation above in terms of signals (only for uncertainties determination and not for reactivity quantification):

$$k_{OH} = \frac{((S3+\Delta S3)-(S2+\Delta S2)}{(S1-(S3+\Delta S3))} \cdot k_p . \frac{S1}{(S_{m19}+X_r.S_{m37}).R_f}.F.D$$

Where, S3, S2, and S1 are the pyrrole signals recorded by the PTR-MS at m/z 68 during the different measurement steps, ΔS3 and ΔS2 changes in pyrrole signals due to the NO interference and changes in relative humidity, respectively, R_F the sensitivity of the PTR-MS to pyrrole, S_{m19} and S_{m37} the signals at m/z 19 (H_3O^+) and m/z 37 ($H_3O^+(H_2O)$), respectively, and X_r the normalization factor to take into account the humidity dependence of the PTR-MS sensitivity (determined experimentally as described by Hansen et al. (2015)).

Making the assumption that the normalization of the pyrrole signal by H_3O^+ and $H_3O^+(H_2O)$ does not bring any supplementary uncertainties, the terms producing uncertainties in the measurements are: S1, S2, S3, ΔS2, ΔS3, k_p, R_f, F, and D.

Assuming that these variables are independent, we can calculate the total uncertainties for OH reactivity measurements using the following equation:

$$U^2_{f(x1,\ldots,xn)} = \int_1^n \left[\left(\frac{\partial f}{\partial xi} \right)^2 .u^2_{xi} \right]$$

Applied to the total OH reactivity measurements, this gives the following equation for the determination of total uncertainty:

$$U^2_{R_{air}} = \left[\frac{(S3+\Delta S3).[(S2+\Delta S2)-(S3+\Delta S3)]}{(S1-(S3+\Delta S3)^2} . \frac{1}{(S_{m19}+X_r.S_{m37})R_f} k_p.F.D \right]^2 .(\sigma^2_{S1})$$

$$+\left[\frac{-1}{(S1-(S3+\Delta S3)} . \frac{S1}{(S_{m19}+X_r.S_{m37})R_f} .k_p.F.D \right]^2 .(\sigma^2_{S2}+\sigma^2_{\Delta S2})$$

$$+\left[\frac{(S1-(S2+\Delta S2))}{(S1-(S3+\Delta S3)^2} . \frac{S1}{(S_{m19}+X_r.S_{m37})R_f} k_p.F.D \right]^2 .(\sigma^2_{S3}+\sigma^2_{\Delta S3})$$

$$+\left[\frac{(S3+\Delta S3)-(S2+\Delta S2)}{(S1-(S3+\Delta S3)} . \frac{S1}{(S_{m19}+X_r.S_{m37})R_f} F.D \right]^2 .(\sigma^2_{kp})$$

$$+\left[\frac{(S3+\Delta S3)-(S2+\Delta S2)}{(S1-(S3+\Delta S3)} . \frac{S1}{(S_{m19}+X_r.S_{m37})R_f} k_p.D \right]^2 .(\sigma^2_{F})$$

$$+\left[\frac{(S3+\Delta S3)-(S2+\Delta S2)}{(S1-(S3+\Delta S3)} . \frac{S1}{(S_{m19}+X_r.S_{m37})R_f} k_p.F \right]^2 .(\sigma^2_{D})$$

$$+\left[-\frac{(S3+\Delta S3)-(S2+\Delta S2)}{(S1-(S3+\Delta S3)} . \frac{S1}{(S_{m19}+X_r.S_{m37})R^2_f} k_p.F.D \right]^2 .(\sigma^2_{Rf})$$

Since the statistic for PTR-MS signals follows a poissonian distribution (De Gouw and Warneke, 2007): $\sigma_{S1} = \sqrt{S1}$, $\sigma_{S2} = \sqrt{S2}$, and $\sigma_{S3} = \sqrt{S3}$. These terms represent the random error (precision) of the measurements. To calculate the precision, it is therefore possible to consider only these three uncertainties as non-zero in the above equations.

The terms leading to a systematic error are: k_p, R_f, F, and D. Their relative uncertainties (1σ) are described below:

- $\frac{\sigma_{kp}}{k_p}$ can be deduced from the literature and is estimated to be 8% (Dillon et al., 2012).
- $\frac{\sigma_{R_f}}{R_f}$ is calculated from the standard deviation of the different pyrrole calibrations performed during the campaigns and in the laboratory, and from the concentration uncertainty on the pyrrole standard (1σ of 5%). The relative uncertainty on the sensitivity is estimated to be 12%.
- $\frac{\sigma_F}{F}$ is calculated from the standard deviation of correction factors obtained for different standard injections upon a restrained range of pyrrole-to-OH ratios (1.4-2.2) assuming that the pyrrole-to-OH dependence of F on this range of ratios is not significant. The corresponding relative uncertainty has been estimated to be 9%.
- $\frac{\sigma_D}{D}$ is calculated from the uncertainties of different flow rates (PTR-MS sampling, reactor exhaust sampling, addition of N_2 and pyrrole) controlled by mass flow controllers (estimated at 1%). The overall relative uncertainty for the dilution correction is estimated to be 2%.

Finally, the uncertainties for ΔS3 and ΔS2 are given below:

- ΔS2 is calculated using the following equation: $\Delta S2 = p\left[\left(\frac{Sm37}{Sm19}\right)_{S3} - \left(\frac{Sm37}{Sm19}\right)_{S2}\right]$ (see equation (3) from the paper), where p is the slope of the relation observed between the pyrrole signal and the m37/m19 ratio. Since the uncertainty on the m37/m19 ratio is negligible (~0.05%), it is assumed that $\frac{\sigma_{\Delta S2}}{\Delta S2}$ depends only on the error associated to the slope determination and is estimated, from laboratory and field experiments, to be 12%.
- ΔS3 is calculated using a quadratic regression of the change in pyrrole signal with NO: $\Delta S3 = a'.NO^2 + b'.NO$. The relative uncertainty on this correction is estimated by propagating the errors on the determination of *a'* and *b'* and the error associated to the NO measurements:

$$\frac{\sigma\Delta S3}{\Delta S3} = \sqrt{\left(\frac{U_{NOmeasurement}}{NO}\right)^2 + \left(U^{rel}_{parametrization}\right)^2}$$

The uncertainty associated to the determination of *a'* and *b'* is estimated using the 1σ confidence intervals of the quadratic regression (see Fig. S14.1). This uncertainty is found to be dependent on the NO mixing ratio.

The uncertainty on NO measurements is estimated using the specification given by the constructor of the NO_x analyzer (Thermo Environmental Instruments, model 42C), i.e. a limit of detection of 0.4 ppb, and a relative precision of 4% determined experimentally.

$$U_{NOmeasurement} = \frac{LOD}{3} + relative.precision * NO$$

The overall estimation of the relative uncertainty for this correction ($\frac{\sigma \Delta S3}{\Delta S3}$) regarding the NO mixing ratio is shown in Fig. S14.2.

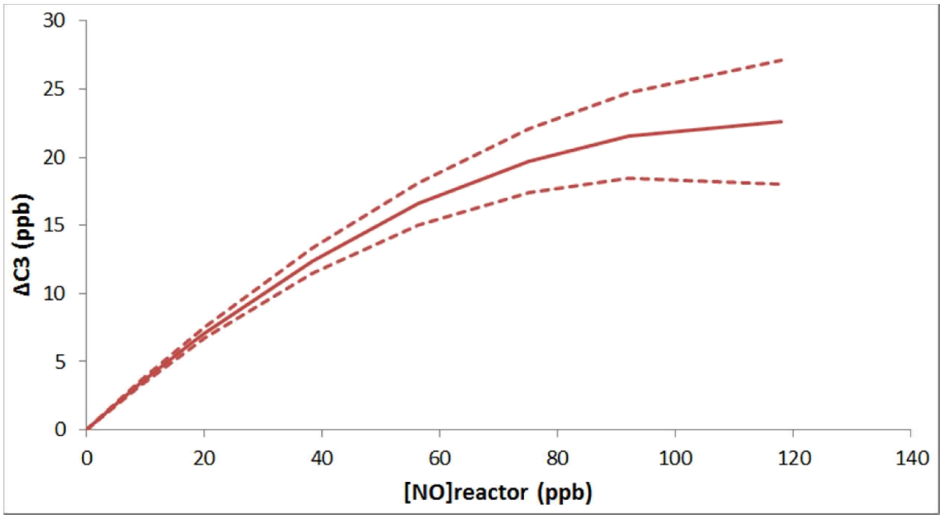

Figure S14.1: Change in C3 as a function of the NO mixing ratio in the reactor. The solid line corresponds to the estimated ΔC3 using the quadratic regression determines experimentally for a pyrrole-to-OH ratio of 3.8, for which the biggest uncertainties are reached. The dashed lines display the 1σ confidence intervals calculated using the errors associated to *a'* and *b'*.

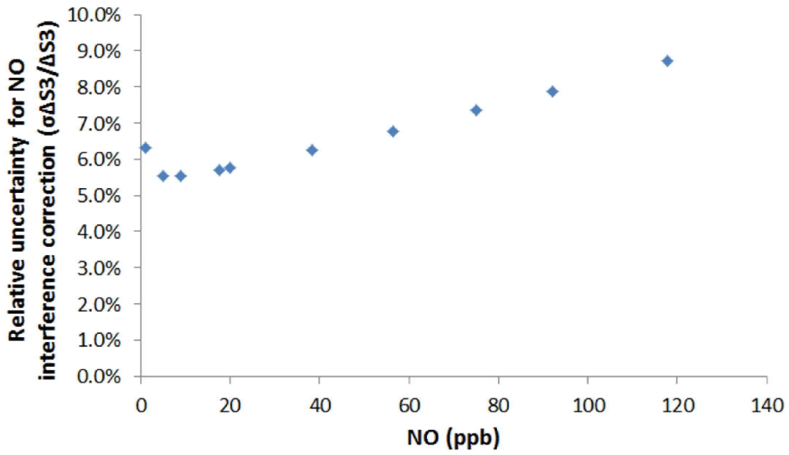

Figure S14.2: Evolution of $\sigma\Delta S3/\Delta S3$ as a function of NO. The relative uncertainty for this correction is estimated by propagating errors associated to the determination of *a'* and *b'* (quadratic regression of ΔC3=f(NO)) and the measurement error on NO.

References

De Gouw, J. and Warneke, C.: Measurements of volatile organic compounds in the Earth's atmosphere using proton-transfer reaction mass spectrometry, Mass Spectrom. Rev., 26, 223–257, 2007.

Dillon, T., Tucceri, M., Dulitz, K., Horowitz, A., Vereecken, L., and Crowley, J.: Reaction of Hydroxyl Radicals with C4H5N (Pyrrole): Temperature and Pressure Dependent Rate Coefficients, J. Phys. Chem. A., 116, 6051–6058, doi:10.1021/jp211241x, 2012

Fittschen, C., Whalley, L. K., Heard, D. E.: The Reaction of CH3O2 Radicals with OH Radicals: A Neglected Sink for CH3O2 in the Remote Atmosphere, Environ. Sci. Technol., 48, 14, 7700-7701, 2014

Hansen, R. F., Blocquet, M., Schoemaecker, C., Léonardis, T., Locoge, N., Fittschen, C., Hanoune, B., Stevens, P. S., Sinha, V., Dusanter, S.: Intercomparison of the Comparative Reactivity Method (CRM) and Pump-Probe technique for measuring total OH reactivity in an urban environment, Atmos. Meas. Tech. Discuss., to be submitted in AMTD, 2015